REPORT DOCUMENTATION PAGE

Form Approved OMB NO. 0704-0188

1. REPORT DATE (DD-MM-YYYY)	2. REPORT TYPE	3. DATES COVERED (From - To)
	New Reprint	-

4. TITLE AND SUBTITLE

Elevated-temperature deformation mechanisms in Ta2C: An experimental study

5a. CONTRACT NUMBER

W911NF-08-1-0300

5b. GRANT NUMBER

5c. PROGRAM ELEMENT NUMBER

611102

6. AUTHORS

Billie Wang, Christopher R. Weinberger, Lawrence E. Matson, Gregory B. Thompson, Nicholas De Leon

5d. PROJECT NUMBER

5e. TASK NUMBER

5f. WORK UNIT NUMBER

7. PERFORMING ORGANIZATION NAMES AND ADDRESSES

University of Alabama - Tuscaloosa
Sponsored Programs
The University of Alabama
Tuscaloosa, AL   35487   -0104

8. PERFORMING ORGANIZATION REPORT NUMBER

9. SPONSORING/MONITORING AGENCY NAME(S) AND ADDRESS(ES)

U.S. Army Research Office
P.O. Box 12211
Research Triangle Park, NC 27709-2211

10. SPONSOR/MONITOR'S ACRONYM(S)

ARO

11. SPONSOR/MONITOR'S REPORT NUMBER(S)

54397-MS.9

12. DISTRIBUTION AVAILIBILITY STATEMENT

Approved for public release; distribution is unlimited.

13. SUPPLEMENTARY NOTES

The views, opinions and/or findings contained in this report are those of the author(s) and should not contrued as an official Department of the Army position, policy or decision, unless so designated by other documentation.

14. ABSTRACT

A polycrystalline a-Ta2C bar, fabricated by hot isostatic pressing, was tested in four-point bending at approximately 1930 $\square$C. The sample showed significant plastic deformation. Transmission electron microscopy, using two-beam defect analysis, confirmed pyramidal dislocation slip of the type $a=3h11\square23if10\square11g$. Basal and prismatic slip of $a=3h11\square20i$ type could not be determined because of significant contrast interference from stacking faults that formed in the material. The increase in stacking fault density observed after thermomechanical

15. SUBJECT TERMS

UHTC; Slip system; Dislocations; TEM; Plastic deformation

16. SECURITY CLASSIFICATION OF:			17. LIMITATION OF ABSTRACT	15. NUMBER OF PAGES	19a. NAME OF RESPONSIBLE PERSON
a. REPORT	b. ABSTRACT	c. THIS PAGE			Gregory Thompson
UU	UU	UU	UU		19b. TELEPHONE NUMBER
					205-348-1589

Standard Form 298 (Rev 8/98)
Prescribed by ANSI Std. Z39.18

Report Title

Elevated-temperature deformation mechanisms in Ta2C: An experimental study

ABSTRACT

A polycrystalline a-Ta2C bar, fabricated by hot isostatic pressing, was tested in four-point bending at approximately 1930 □C. The sample showed significant plastic deformation. Transmission electron microscopy, using two-beam defect analysis, confirmed pyramidal dislocation slip of the type a=3h11□23if10□11g. Basal and prismatic slip of a=3h11□20i type could not be determined because of significant contrast interference from stacking faults that formed in the material. The increase in stacking fault density observed after thermomechanical loading is not believed to be caused by deformation but rather is due to growth faults that formed from the slight carburization of Ta2C from the graphite heating filaments in the testing apparatus. The significant plasticity accommodation in Ta2C is a result of basal and non-basal slip and the wide spacing of the Ta–Ta metallic bonds that form inherent to its crystallography.

REPORT DOCUMENTATION PAGE (SF298)
(Continuation Sheet)

Continuation for Block 13

ARO Report Number   54397.9-MS
Elevated-temperature deformation mechanisms   ...

Elevated-temperature deformation mechanisms in Ta₂C: An experimental study

Nicholas De Leon [a], Billie Wang [a], Christopher R. Weinberger [b], Lawrence E. Matson [c], Gregory B. Thompson [a,*]

[a] *The University of Alabama, Department of Metallurgical & Materials Engineering, Box 870202, Tuscaloosa, AL 35401-0202, USA*
[b] *Sandia National Laboratories, Albuquerque, NM 87185-1411, USA*
[c] *Air Force Research Laboratory, Materials and Manufacturing Directorate, RXCC Building 655, Room 186, 2230 Tenth St., Wright-Patterson AFB, OH 45433-7817, USA*

Abstract

A polycrystalline α-Ta₂C bar, fabricated by hot isostatic pressing, was tested in four-point bending at approximately 1930 °C. The sample showed significant plastic deformation. Transmission electron microscopy, using two-beam defect analysis, confirmed pyramidal dislocation slip of the type $a/3\langle11\bar{2}3\rangle\{10\bar{1}1\}$. Basal and prismatic slip of $a/3\langle11\bar{2}0\rangle$ type could not be determined because of significant contrast interference from stacking faults that formed in the material. The increase in stacking fault density observed after thermomechanical loading is not believed to be caused by deformation but rather is due to growth faults that formed from the slight carburization of Ta₂C from the graphite heating filaments in the testing apparatus. The significant plasticity accommodation in Ta₂C is a result of basal and non-basal slip and the wide spacing of the Ta–Ta metallic bonds that form inherent to its crystallography.
© 2013 Acta Materialia Inc. Published by Elsevier Ltd. All rights reserved.

Keywords: UHTC; Slip system; Dislocations; TEM; Plastic deformation

1. Introduction

The tantalum carbide system is known for its ultrahigh melting temperature and high hardness [1]. As a result, tantalum carbides have found uses in a variety of wear-resistant applications including machine tooling, coatings for injection molding of aluminum alloys, and brake liners [2–4]. An interesting attribute of the tantalum carbides is the duality in mechanical properties they exhibit. At temperatures <~1000 °C, the system, in general, exhibits classic hard and brittle behavior common to ceramics. At elevated temperatures equal to or greater than approximately one-third to one-half the melting temperature, T_m, there is a brittle-to-ductile transition (BDT) [5] and this carbide system can exhibit significant plastic behavior. The ductility of the TaC phase has been reported to be as high as 33% [6]. Of all the Group V carbides, the tantalum carbides have been reported to exhibit the most metallic character [1]. This may explain the ability for these phases to be more ductile at elevated temperatures.

Carbides, like some other ceramic systems [7], deform plastically at room temperature via dislocations under indentation. This indicates that dislocation energies and mobility, even at these lower temperatures, are not prohibitive. Kim et al. [8], using room-temperature indentation studies, have shown through transmission electron microscopy (TEM) that dislocation loops form in the γ-TaC phase under the indenter. Within these loops, the higher-mobility $a/2\langle110\rangle$ edge dislocations glide on {111} planes and annihilate at the crystal interfaces within the microstructure. This leaves less mobile, long screw dislocations from the loop within the grains. The presence of these

* Corresponding author. Tel.: +1 205 348 1589; fax: +1 205 348 2164.
  E-mail address: gthompson@eng.ua.edu (G.B. Thompson).

stalled screws and the propensity for slip via edge-segment dislocations suggests that lattice friction limits screw mobility, which, in turn, inhibits plastic deformation at low temperatures.

Since TaC has the B1 crystal structure [1,9], which is a face-centered cubic (fcc) Ta atom lattice with the C atoms occupying the octahedral interstitial sites (Fig. 1a), this type of slip could be anticipated as it is also common to fcc metals. Similar to fcc metals, these dislocations may disassociate into Shockley partials. The motion of partial dislocations in the TaC B1 structure requires the motion of either neighboring metal atoms over one another or the motion of a metal atom over a carbon atom. The latter process, in which it is assumed the motion of the metal atom over the carbon atom is energetically unfavorable, requires the coordinated motion of the carbon atoms to an alternate stacking location and is termed the "synchro-shear" process [10–12]. In the context of the synchro-shear mechanism, it is most often assumed that the carbon atoms diffuse through the dislocation core, resulting in dislocation motion being limited by carbon diffusion. However, a similar motion can be achieved by the passage of another Shockley partial on an adjacent plane; the pair is termed a zonal dislocation. All of the above scenarios result in large frictional forces for dislocation glide. As TaC_{1-x} becomes sub-stoichiometric, the carbon content is reduced and the site occupancy is lowered, making the Peierls stress a function of carbon content [11].

At elevated temperatures thermal activation further reduces the lattice resistance during slip. This allows TaC to deform readily via mixed dislocations [8]. This suggests that lattice friction controls plasticity at low to intermediate temperatures and the BDT is most likely caused by the thermally activated glide of screw dislocations at elevated temperatures [8,11].

Slip system studies of other transition metal monocarbides have shown propensities for $\langle 1\,1\,0\rangle\{1\,1\,0\}$ [10] and $\langle 1\,1\,0\rangle\{1\,1\,1\}$ slip [13,14]. The change in slip systems across the transition metal monocarbides may reflect that change in the relative contributions of the mixed covalent–ionic–metallic bonding character within these materials and highlights the importance of directional bonding.

While the TaC phase has been the subject of some deformation mechanism studies in the tantalum carbide system [5,8], the trigonal α-Ta_2C system (often hexagonal in the literature) has received little to no investigation. This results in a great opportunity to understand plasticity in α-Ta_2C specifically, and in transition metal hemicarbides (M_2C) in general. Ta_2C undergoes an allotropic phase transformation near 2000 °C from the trigonal α phase, which is C6, or the CdI_2 antitype structure [15,16,29], to the hexagonal β phase, which is the $L'3$ structure [1]. The major difference between the α and β phases is that the carbon sub-lattice disorders for the high-temperature β phase. In the α phase, the Ta atoms occupy the close-packed hexagonal lattice and the C atoms fill every other plane of the octahedral spaces between the close-packed layers (see Fig. 1b). In the β phase, the Ta atoms occupy the same sites, but the C atoms now occupy all the octahedral interstices with equal one-half probability. This particular stacking sequence allows for a mixture of bonding character, with both strong covalent–ionic bonding between Ta–C layers and metallic bonding between the Ta–Ta, which introduces the potential for even more metallic behavior to exist in this carbide. Considering the crystallography of this phase, which does not offer five independent easy slip systems (as with the fcc-like structures), the competition between the local metallic bond and the orientation of the crystal plane provides an interesting opportunity to understand how Ta_2C deforms as compared to the fcc-like covalently bonded TaC phase.

This paper addresses an experimental investigation of the thermomechanical mechanisms in Ta_2C. Elucidating the dislocation behavior provides the necessary insights to develop strategies that may improve the ductility within tantalum carbides. A companion paper [17], which describes a first-principles investigation, provides computational findings that support the experimental results of this work.

2. Experimental

2.1. Sample fabrication

The Ta_2C test bars were produced by Exothermics, Inc. by mixing constituent TaC and Ta powder at the
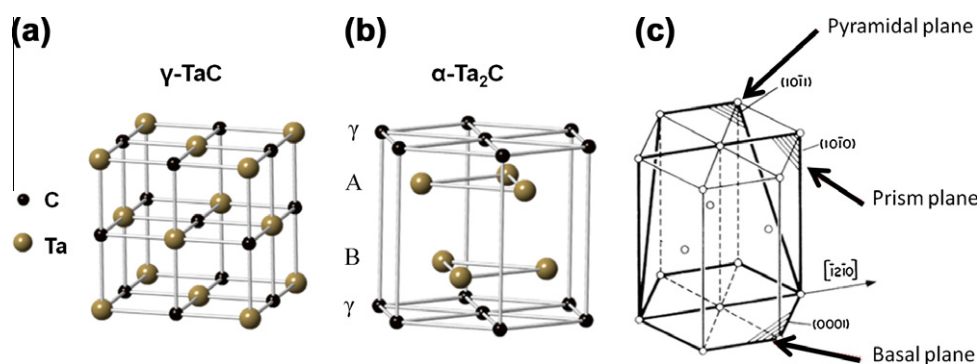

Fig. 1. (a) TaC rock salt crystal structure. (b) Ta_2C crystal structure with stacking sequence noted using Roman letters for the metallic layers and Greek letters for the carbon layers. (c) Slip planes in the hexagonal type structure.
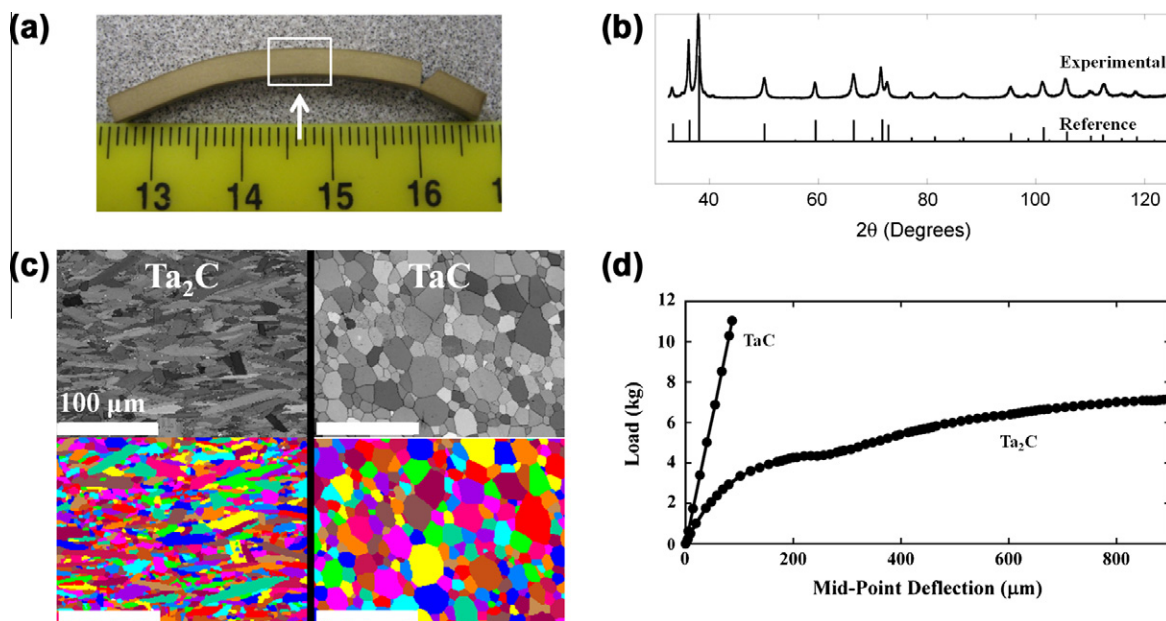
Fig. 2. (a) Post-test sample bar. Significant bar bending was observed. (The crack on the right side of the image occurred during specimen preparation after thermomechanical testing.) (b) XRD scan of Ta_2C specimen tested at 1930 °C and compared to Ref. [13]. (c) SEM-EBSD showing the average grain sizes of Ta_2C and TaC. (d) Mid-point deflection for Ta_2C and TaC at 1930 °C.

appropriate weight fractions. The powders were mechanically pressed and evacuated in a Ta container referred to as a "can". The can was subjected to hot isostatic pressing (HIP) at 200 MPa and 1600 °C for 100 min in an argon atmosphere. The Ta can was mechanically machined away from the HIP billet. In addition, the near surface of the billet was mechanically ground to remove any possible interdiffusion reaction zone between the consolidated Ta_2C powders and the Ta can. The post-HIP billet had a density of ~98% measured by a water emersion displacement technique and compared to the theoretical density of 14.8 g cm^{-3} for Ta_2C [18]. A single-phase TaC billet was also prepared under similar conditions and is included in this work to provide a benchmark mechanical response comparison to Ta_2C. Further details on the microstructure and HIP processing can be found in Ref. [19].

2.2. Mechanical testing

The HIPed billets was machined into 3 mm × 4 mm × 45 mm test bars and mechanically tested at ~1930 °C (3500 °F) according to the modified specifications provided in MIL-STD-1942A [20]. The four-point flexural testing apparatus was housed in a resistively heated graphite element furnace and, to reduce oxidation and (de)carburization effects, ultrahigh-purity argon gas was flowed over the specimen during testing. X-ray diffraction (XRD), using a Bruker Discovery D8 General Area Diffraction System (GADDS) XRD operated with Cu Kα radiation (1.5405 Å) at 45 keV and 40 mA, was used to determine the phase content in the test bar pre/post-testing.

2.3. Microscopy preparation

Cross-sections were sliced from the central region of the Ta_2C test bar where maximum bending occurred (Fig. 2a). These slices were mounted and mechanically ground and polished using a combination of SiC and diamond abrasives with a final aqueous 0.05 μm silica slurry Vibromet® polish. Specimens for scanning electron microscopy (SEM) were mounted in a conductive epoxy for handling. TEM foils were prepared by ultrasonically drilling 3 mm discs from the cross-sections using a Fischione Instruments Model 170 drill with a SiC abrasive slurry. The discs were then mechanically ground to <100 μm using SiC and then dimpled to <15 μm with 6 μm diamond paste polish under a rotating 15 mm diameter steel wheel using a Fischione Instruments Model 200 unit. The dimpled discs were argon ion milled to electron transparency using a Gatan Precision Ion Polishing System (PIPS®). The PIPS® dual guns were operated at 3 keV per gun and aligned at contrary incident milling angles of 8° to achieve perforation. The guns were operated at 2 keV and 6° for a final "clean-up" step. The specimens were continuously rotated during the ion milling.

2.4. Electron microscopy

Electron backscattered diffraction (EBSD) SEM images were collected using an Oxford-HKL Nordlys platform attached to a JEOL 7000F field emission microscope. The EBSD patterns were collected at 30 keV with a 90 μA emission current (150 pA contacting the sample) at a frame capture rate of 42 frames s^{-1}.

Conventional dynamic TEM was performed with a FEI F20 Tecnai (S)TEM and a Philips CM200, both operated at 200 keV. High-resolution TEM (HRTEM) was performed using a C_s-aberration-corrected FEI Titan (S)TEM operated at 300 keV. The Burgers vectors were determined by conventional $\mathbf{g} \cdot \mathbf{b} \times \mathbf{u}$ analysis, where $\mathbf{g}$ is the diffraction vector, $\mathbf{b}$ is the Burgers vector of the dislocation and $\mathbf{u}$ is the line sense of the dislocation [21].

HRTEM simulation images were generated using Kirkland's TEMSIM program package [22]. The simulation is based upon the multi-slice method in which the structure is decomposed into atomic-layered sections for the appropriate viewing direction. These combined slices have both chemical and spatial information that are used in the electron interaction equations to determine contrast according to the microscope imaging parameters. Slices were created for a $[11\bar{2}0]$ viewing direction and stacked for a sample thickness of 10 nm.

3. Results

3.1. Phase identification

The XRD spectrum, shown in Fig. 2b, of the elevated Ta_2C test bar was consistently indexed to the α-Ta_2C phase, i.e. no oxidation or other carbide phases were detected. Electron diffraction, shown later, also did not reveal any other phases and is consistent with the XRD data.

3.2. Grain size analysis

The SEM-EBSD images revealed that the TaC and Ta_2C had an average grain size of 21 and 13 μm, respectively, as shown in Fig. 2c.

3.3. Mechanical bending tests

The load vs. mid-point deflection plot for a Ta_2C bar is shown in Fig. 2d. For comparison, the TaC test bar is plotted on the same graph. The Ta_2C specimen exhibits significantly more plasticity compared to the TaC test bar as evident by its greater deflection.

3.4. Dislocation analysis

Typical dislocation structures observed in the Ta_2C foils can be seen in the bright-field (BF) TEM micrographs of Fig. 3. Dense forest dislocation structures were observed when viewed looking down the $[0001]$ zone axis (Fig. 3a), while terminating dislocations and dislocations running parallel with the basal plane were visible when viewed from the $[11\bar{2}0]$ axis or edge onto the basal plane (Fig. 3b). In addition, what appeared to be a Frank–Read
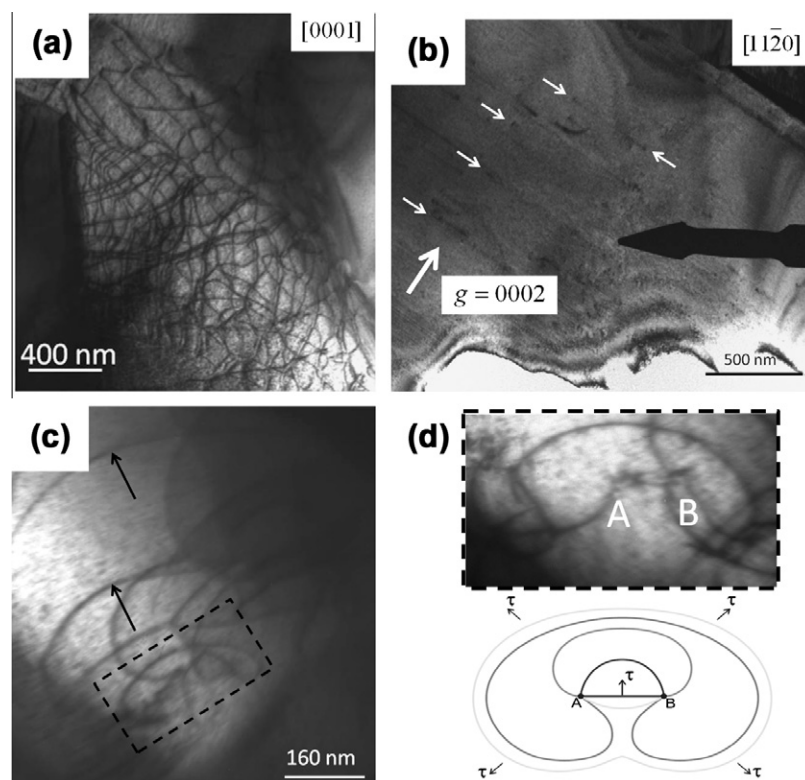

Fig. 3. BF-TEM dislocations. (a) Dense forest-like dislocations viewed from the $[0001]$ zone axis. (b) Dislocations, indicated by white arrows, viewed using $\mathbf{g} = (000\bar{2})$. (c) Frank–Read source operating in Ta_2C. The arrows indicate dislocations that have bowed out from the source. (d) A high-magnification image, taken from the dashed box in (c), and a schematic of a Frank–Read source with "A" and "B" as the pinning locations.

source was also observed in this system (Fig. 3c and d). The pinning locations can be seen in the detailed image while the bowed-out dislocations are observed gliding outwards, as indicated by the arrows in Fig. 3c.

In the presented imaging analysis, two dislocations were considered and characterized using the conventional two-beam $\mathbf{g} \cdot \mathbf{b} \times \mathbf{u}$ technique. In Fig. 4a, the dislocations are clearly visible using the $(\bar{1}\bar{1}20)$ reflection condition taken from the $[0001]$ zone axis. Upon tilting to the $(\bar{2}\bar{2}4\bar{2}), (2\bar{1}\bar{1}2)$, and $(\bar{1}3\bar{2}\bar{1})$ reflections, the dislocations become invisible (Fig. 4b–d). The inset images in Fig. 4 are the two-beam diffraction conditions for each respective image. The consistent Burgers vector identified under these imaging conditions for the dislocations is of the $\langle c + a \rangle$ type, $\mathbf{b} = a/3[\bar{2}113]$. Slip with this Burgers vector and these imaging conditions was stereographically determined to be on the $(1\bar{1}01)$ pyramidal plane. This dislocation slip was again confirmed using a different set of dislocations (not shown). Basal plane slip was not quantitatively confirmed because of contrast interference caused by a high density of stacking faults on the basal plane, which will be discussed below.

3.5. Stacking faults

The mechanically deformed specimen exhibited a significant number of faults as seen in Fig. 5. Using $(0\bar{1}12)$ and $(0\bar{1}11)$ reflections from the $[11\bar{2}0]$ zone, the outer band contrast of each fault, indicated by the arrows in Fig. 5,

does not invert, i.e. dark remains dark. This contrast experiment relies on the use of reflections (h, k, i, l) that fulfill the condition $h - k = 3n \pm 1$, where $n = 0, \pm 1, \pm 2$, etc. and only l is varied as even or odd [23,24]. The lack of a contrast inversion for the outer band is indicative of an intrinsic I_2 fault. An I_2 fault is achieved by pure shear of the basal stacking sequence in hexagonal close-packed (hcp) materials [25]. However, α-Ta$_2$C is trigonal with two atomic species, one of which has a hcp structure. This can complicate the interpretation of the contrast images as will be presented in the Discussion below.

The change in the stacking sequence for these stacking faults can also be observed in the HRTEM images, acquired using the $[11\bar{2}0]$ zone axis, shown in Fig. 5a. The expected close-packed stacking sequence for Ta$_2$C would be γABγABγABγ, where Latin letters represent the metallic layers and Greek letters represent the carbon layers [26], as seen in Fig. 1b. The bright-to-bright spherical contrast spacing was measured to be 4.94 Å in Fig. 5a, which agrees reasonably well with the previously reported **c** parameter of Ta$_2$C, 4.95 Å [16]. The brighter spherical contrast spots are denoted as B layers and the faint spherical contrast seen between are the A layers. Since Ta has a much larger scattering potential than C [11], it generates the apparent, distinct contrast, whereas the carbon layers were more diffusely scattered and not visible. This was confirmed by the simulated HRTEM image of Fig. 5b. Considering the diffuse scattering of carbon, only the metallic layers, represented by the Roman letters, are marked in
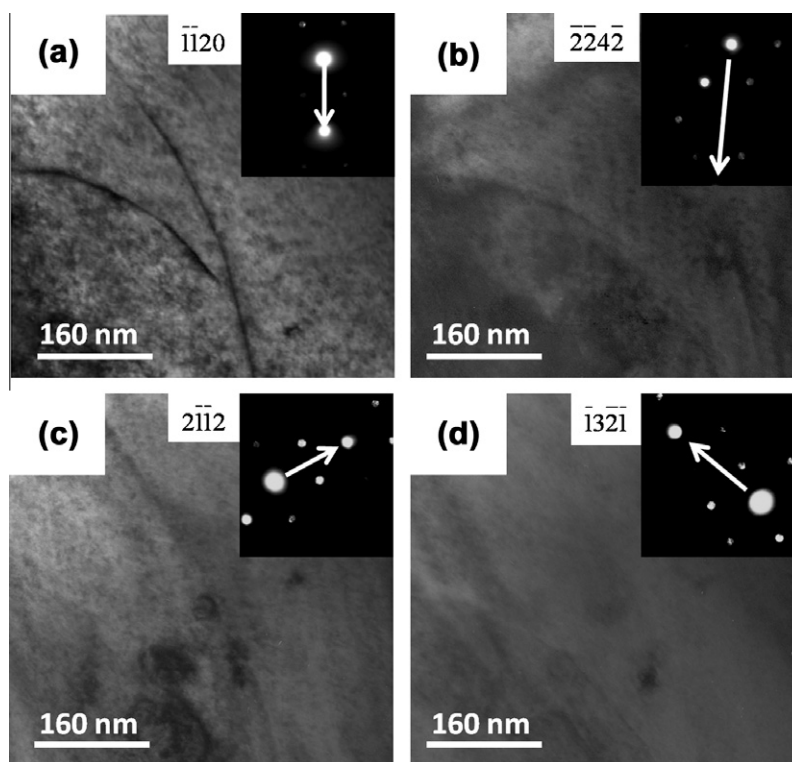

Fig. 4. BF-TEM images with associated two-beam conditions in the inset. (a) Pyramidal dislocations clearly visible with $g = (\bar{1}\bar{1}20)$ and invisible with (b) $g = (\bar{2}\bar{2}4\bar{2})$, (c) $g = (2\bar{1}\bar{1}2)$, and (d) $g = (\bar{1}3\bar{2}\bar{1})$.
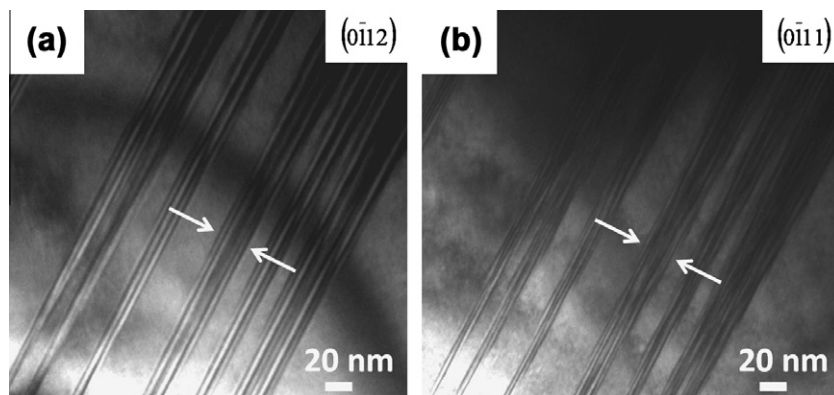
Fig. 5. I$_2$ faulting. (a) Dark outer fringes, indicated by arrows, visible when *l* is even. (b) Outer fringe, indicated by equivalent arrows in (a), where the contrast does not invert when *l* is odd.

each of the images. The nominal hcp stacking of just the metal basal planes, having removed the visibility of carbon, is now ABABABABAB. Upon passing an I$_2$ intrinsic fault, the resultant stacking sequence is ABABA|CBCBC [25] and can be observed in the HRTEM images. This is consistent with the previous, conventional two-beam-determined I$_2$ fault images seen in Fig. 4. However, it is important to note that since the C atoms do not contribute to HRTEM images, the local carbon ordering, or local composition, cannot be determined.

Since the viewing conditions to yield visibility and invisibility conditions for the basal and prism planes' dislocations rely on similar imaging conditions to those used for the faults, it was not possible to discern images where the dislocations were clearly apparent with the corresponding contrast of the fault on the basal plane. For example, in Fig. 3b, dislocations are seen on the basal plane. The strong contrast of these dislocations suggests that these are not of the $a/3[11\bar{2}0]$ type considering that the imaging $\mathbf{g}$ vector would yield an invisible condition for such a dislocation, i.e. $\mathbf{g} \cdot \mathbf{b} = 0$. Contrast can exist under a $\mathbf{g} \cdot \mathbf{b} = 0$ condition for edge or mix dislocations because of the cross-product of $\mathbf{g}$ and the line sense, $\mathbf{u}$, but would be very weak. Hence, these dislocations shown in Fig. 4b must be the intersection of the dislocation line from another plane onto the basal plane.

4. Discussion

It is interesting to see that the plastic deformation of Ta$_2$C is much larger than that of monocarbide TaC, as shown in Fig. 2d. In comparison with close-packed metals, the fcc structure is generally more ductile than a hcp structure because the fcc structure has a larger number of available close-packed planes [27], e.g. four variants of $\{111\}_{fcc}$ planes vs. one basal $\{0001\}_{hcp}$ plane. For general plastic deformation by slip in polycrystalline materials, five independent plastic degrees of freedom are required [25]. In fcc crystals, this is met by the 12 standard $\langle 110 \rangle \{111\}$ slip systems. In hexagonal and trigonal materials, easy glide on

the single (0001) basal planes provides only two independent slip systems via $\langle 11\bar{2}0 \rangle$ perfect dislocations. When slip occurs on the prism planes via $\langle 11\bar{2}0 \rangle$, this adds two additional slip systems. To achieve the five degrees of freedom, either slip via $\langle 0001 \rangle$ dislocations on the prism planes or slip via $\langle 11\bar{2}3 \rangle$ dislocations on pyramidal planes must occur. Once one of these latter slip systems is initiated, the trigonal and hexagonal structures meet the von Mises criteria for general plastic deformation. Considering these challenges, one might initially be surprised that the trigonal Ta$_2$C phase shows more plasticity than the fcc-based TaC phase.

Another possible explanation for observed differences are the large discrepancies in the grain size between the two bending specimens. It is well known that the strength of a material depends on the average grain size through the Hall–Petch relationship, and, if the TaC bar has much smaller grains than the Ta$_2$C bar, then plastic flow would occur much later in the TaC specimen. However, our EBSD scans show similar grain sizes even if the grain structures (acicular vs. equiaxed) are somewhat different (Fig. 2c). This suggests that the differences observed in the plastic deformation are not caused by a simple difference in grain sizes but are probably inherent to the materials themselves.

If the differences in plastic deformation are not caused by grain size effects and cannot be easily explained by the number of available slip systems, the difference is probably caused by the difference in the bonding of the two materials. We note that the materials are deformed at slightly different homologous temperatures as TaC melts at ∼3900 °C and Ta$_2$C melts at ∼3300 °C [1], which corresponds to deformation at homologous temperatures of 0.53 and 0.62, respectively. While this does give a broad explanation of our observations, it does not explain the nature of the change in bonding that gives rise to the dramatic differences observed in the plastic deformation.

The most compelling and complete explanation of the differences in plastic deformation are detailed in a companion theoretical paper [17] which shows that slip is easier
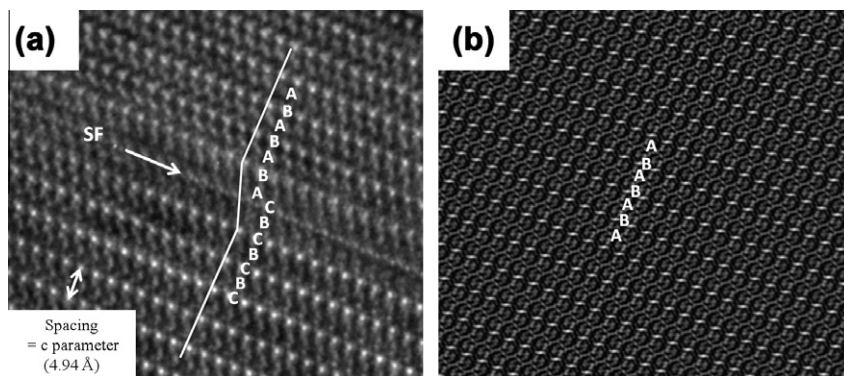
Fig. 6. (a) HRTEM stacking fault as viewed down $[11\bar{2}0]$ zone axis, with inset lattice spacing measurement. (b) HRTEM simulation with stacking sequences labeled.

between the metal–metal layers in Ta_2C. This work furthermore shows that slip is most likely to occur between the metal–metal layers of the basal plane followed by slip between the metal–metal layers on one of the pyramidal planes. Assuming the most of the plastic deformation occurs by slip between the basal planes in Ta_2C and $\{111\}$ planes in TaC, we can better understand the enhanced ductility in Ta_2C. Slip on the $\{111\}$ planes in TaC is similar to slip between the Ta–C layers in Ta_2C since they have similar bonding and interplanar spacing [1,15–17]. As shown in [17], the generalized stacking fault energy surfaces for Ta–Ta layers in Ta_2C are much lower than those between Ta–C layers, making slip between Ta–C layers much more difficult. Thus, slip on the basal plane between metal layers is much easier than slip between Ta–C layers in TaC, and hence more plasticity occurs in Ta_2C.

The above argument for the enhanced plasticity in α-Ta_2C relies on the assumption that basal slip is dominant. However, in hcp metals, the competition between slip on the basal and prism plane is related to the interplanar spacing, which is equal at the ideal c/a ratio of 1.633 [25]. For materials with larger c/a ratios, basal slip is preferred because it has a larger spacing, while lower c/a ratios would more easily accommodate prism slip. For α-Ta_2C, the c/a ratio is 1.59, which suggests it may be favorable for prismatic slip. However, a detailed analysis in our companion paper shows that, based on the α-Ta_2C crystal structure, the largest interplanar spacing occurs between the Ta–Ta layers on the basal plane and that the prism spacing is quite small.

Unfortunately, no dislocations were reliably observed on the basal or prism planes in our experiments. The ideal Burgers vector for slip on these planes would be $\mathbf{b} = a/3\langle11\bar{2}0\rangle$ and the observed basal plane stacking faults share these directions. As noted previously, attempts to view dislocations using diffraction vectors that would allow $\mathbf{b} = a/3\langle11\bar{2}0\rangle$ visibility, such as $(\bar{1}013)$, resulted in images completely dominated by the stacking fault contrast (Fig. 5), and the line defect could not be readily seen. This problem precludes the use of the traditional two-beam $\mathbf{g} \cdot \mathbf{b}$ technique to define the basal and prismatic slip systems.

Our inability to image basal or prismatic dislocations highlights the utility of coupling these experiments to theory. In the companion paper [17], first-principles density function theory calculations predict that basal slip is the most energetically favorable slip system. An experimental study into the W_2C system, which also has the CdI_2 structure with a less than ideal c/a ratio, showed only basal slip [28]. Thus, we expect to see basal slip as the dominant deformation mechanism when faulting is not present to obscure the necessary viewing angles. The next most favorable slip was calculated to be pyramidal slip between Ta–Ta layers.

Slip on a pyramidal plane (Fig. 4) was observed, confirming that $\langle c + a \rangle$ dislocations do occur to accommodate the deformation. Pyramidal slip has also been observed to operate in hexagonal symmetry materials as a mode of secondary slip, occurring on the $(10\bar{1}1)$ and $(11\bar{2}2)$ planes, the choice of which is temperature and material dependent [25]. The secondary slip system discovered in this study is of the $a/3\langle11\bar{2}3\rangle\{10\bar{1}1\}$ or $a/3\langle11\bar{2}3\rangle\{10\bar{1}\bar{1}\}$ type, and the differences between the two pyramidal planes cannot be determined. This agrees well with our theoretical predictions. The high deformation temperature, polycrystalline nature of the sample and the imposed bending deformation all likely enhanced the propensity for non-basal slip.

This specimen showed a high density of faulting, which, as noted above, obscures our ability to image basal dislocations. TEM analysis of a non-deformed Ta_2C specimen did not show, qualitatively, a significant number of faults as compared to the deformed specimen (Fig. 7). Based upon those observations, it could be rationalized that these structures were deformation induced. In the companion paper [17], the intrinsic stacking fault energy on the basal plane between the Ta–Ta layers and the Ta–C layers was approximately ~1 and ~4 $J\,m^{-2}$, respectively [17]. These intrinsic stacking fault energies, which are quite high, suggest that deformation faulting is an unlikely deformation mechanism in this material. Furthermore, we note [17] that the difference between the intrinsic fault and unstable energies between the Ta–Ta layers is small, suggesting that deformation faults would be relatively unstable in Ta_2C. However, the two-beam diffraction contrast images of the
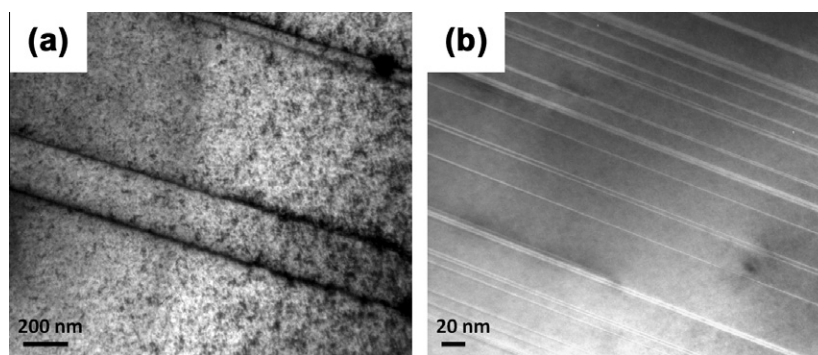
Fig. 7. (a) BF-TEM stacking faults in non-deformed Ta_2C viewed down the $[11\bar{2}0]$ zone axis. (b) BF-TEM stacking faults in deformed Ta_2C viewed down the $[11\bar{2}0]$ zone axis deformed Ta_2C. Note the qualitative increase in faulting after testing.

Table 1
Atomic percentage of carbon content pre- and post-testing as measured by LECO combustion infrared absorption analysis.

	C (at.%)
Non-deformed	27.95
Deformed	33.95

faults (Fig. 5) and the stacking sequences observed in the HRTEM image (Fig. 6) suggest a shift in the stacking of the Ta atoms. It is possible that these faults are not pure deformation (shear) faults but correspond to a local change in composition, which would stabilize the fault.

LECO combustion and infrared analysis [29] of the carbon content of non-deformed and deformed samples is listed in Table 1. During testing, the Ta_2C sample gained $\sim$6 at.% C. This carbon uptake is attributed to the use of a graphite furnace during thermal–mechanical testing. The additional carbon, with enhanced mobility from being near the α-to-β disordering temperature, would result in a local composition change and the formation of crystallographic shear planes, similar to what is observed in non-stoichiometric oxides [30]. In addition, the post-tested carbon content places the overall composition within the Ta_2C and Ta_4C_3 phase field, though the volume fraction of Ta_4C_3 would be negligible, as confirmed by the lack of XRD and electron diffraction of this phase. The precipitation of Ta_4C_3 from Ta_2C has been shown to occur off the basal plane [19]. The introduction of additional carbon layers on the basal plane is consistent with where the carbon-rich phase would nucleate. The placement of excess carbon on the basal plane would create a carbon-rich region which would prefer to stack itself like the fcc TaC phase: γAB-γABγABγ → γABγA|β|CαBCα, or ABABA|CBCBC considering the invisibility of carbon in the HRTEM image (Fig. 6). The presence of this local fcc character would result in a stacking sequence equivalent to what an I_2 fault would induce, as shown earlier, and thus behave in the same way in contrast experiments, like the ones performed in Figs. 5 and 6, and not be differentiable from each other. Thus, the faults seen in these experiments are not believed

to be deformation induced but rather growth induced because of excess carbon gained during the testing of the material.

The ability for Ta_2C to exhibit both basal and non-basal slip allows the system to accommodate general plastic deformation. As discussed in Ref. [17], twinning, often observed in hcp materials, is unlikely to occur in Ta_2C because it would require the passage of twinning dislocations between the Ta–C layer, which is energetically unfavorable, and therefore general plastic deformation should be accommodated primarily through slip via perfect dislocations. In addition, the localized, more metallic and wider-spaced Ta–Ta bonds dictate which Ta_2C planes are dominant in accommodating that deformation. The presence of such bonds, which are absent in TaC, contribute to Ta_2C having greater plasticity (Fig. 2d). Clearly, the lack of carbon in these Ta–Ta close-packed planes reduces the resistance to slip and eliminates the need for the "synchro-shear" slip process that is theorized to occur in the TaC system [10–12].

5. Conclusion

Ta_2C exhibits significantly more plastic deformation than TaC at 1930 °C. This increased deformation accommodation was achieved through basal and non-basal slip. Unfortunately, basal and prismatic slip of the $a/3\langle11\bar{2}0\rangle$ type could not be determined because of contrast interference caused by a high density of stacking faults. Pyramidal slip of the $a/3\langle\bar{2}113\rangle\{1\bar{1}01\}$ type was observed. A companion paper on the generalized stacking fault energies [17] revealed that the pyramidal slip is energetically more favorable than prismatic slip due to the wider spacing in the pyramidal plane, a feature of the particular crystal structure. This has been attributed to the local metallic Ta–Ta layers that exist in this crystallographic phase. The stacking faults were confirmed to be intrinsic I_2 faults and are not believed to be a result of deformation. Rather, they are crystallographic shear planes or growth faults from the early onset of Ta_4C_3 precipitation. The excess carbon source was from the off-gassing from the graphite heating filaments associated with the mechanical testing apparatus. In summary, the ability to access multiple

deformation slip planes, and in particular the local metallic bonding character, allowed enhanced plasticity to occur in Ta_2C.

References

[1] Storms EK. The tantalum–tantalum carbide system. In: The refractory carbides. New York: Academic Press; 1967.
[2] Wang CR, Yang JM, Hoffman W. Mater Chem Phys 2002;74:272.
[3] Upadhyay K, Yang JM, Hoffman WP. Am Ceram Soc Bull 1997;76:51.
[4] Balani K, Gonzalez G, Agarwal A, Hickman R, O'Dell JS. J Am Ceram Soc 2006;89:1419.
[5] Kelly A, Rowcliffe DJ. J Am Ceram Soc 1967;50:253.
[6] Steinitz R. Mechanical properties of refractory carbides at high temperature. In: Boltax A, Handwerk JH, editors. Nuclear applications of non-fissionable ceramics. La Grange Park, IL: American Nuclear Society; 1966.
[7] Ghosh D, Subhash G, Bourne GR. Sci Mater 2009;61:1075.
[8] Kim C, Gottstein G, Grummon DS. Acta Metall Mater 1994;42:2291.
[9] Santoro G, Probst HB. An explanation of microstructures in the tantalum–carbon. system. In: Mueller WM, Mallett G, Fay M, editors. Advances in X-ray analysis: proceedings of the 12th annual conference on applications of X-ray analysis. New York: Plenum Press; 1963.
[10] Hollox GE. Mater Sci Eng 1968;3:121.
[11] Lewis MH, Billingham J, Bell PS. Non-stoichiometry in ceramic compounds. In: Thomas G, Fulrath R, Fisher RM, editors. Electron microscopy and structure of materials. Proceedings of the 5th international materials symposium. Berkeley: University of California Press; 1971.
[12] Rowcliffe DJ. Deformation of ceramic materials II. In: Tressler RE, Bradt RC, editors. Mater Sci Res 1983;18:49.
[13] Rowcliffe DJ, Hollox GE. J Mater Sci 1971;6:1261.
[14] Morgan G, Lewis MH. J Mater Sci 1974;9:349.
[15] Lonnberg B, Lundstrom T, Tellgren R. J Less-Common Met 1986;120:239.
[16] Bowman AL, Wallace TC, Yarnell JL, Wenzel RG, Storms EK. Acta Crystallogr 1965;19:6.
[17] Wang B, De Leon N, Weinberger CR, Thompson GB. Acta Mater (2013), in press. http://dx.doi.org/10.1016/j.actamat.2013.01.047.
[18] Rudy E, Harmon DP. AFML-TR-65-2, Part I, vol. V. Air Force Materials Laboratory Research and Technology Division, Air Force Command, Wright-Patterson AFB, OH; 1965.
[19] Morris RA, Wang B, Matson LE, Thompson GB. Acta Mater 2012;60:139.
[20] MIL-STD-1942A. Flexural strength of high performance ceramics at ambient temperature. Army Materials and Mechanics Research Center (AMMRC), Department of the Army; 1991.
[21] Edington JW. Practical electron microscopy in material science. Eindhoven: Philips' Gloeilampenfabrieken; 1976.
[22] Kirkland EJ. Advanced computing in electron, microscopy; 1998.
[23] Blank H, Delavignette P, Gevers R, Amelinckx S. Phys Status Solidi 1964;7:747.
[24] Hitzenberger C, Karnthaler HP, Korner A. Phys Status Solidi A 1985;89:133.
[25] Hirth JP, Lothe J. Theory of dislocations. second ed. Malaba, FL: Krieger; 1982.
[26] Rowcliffe DJ, Thomas G. Mater Sci Eng 1975;18:231.
[27] Groves GW, Kelly A. Philos Mag 1963;8:877.
[28] Epicier T, Esnouf C, Dubois J, Fantozzi G. Scr Metall 1981;15:1279.
[29] Northern Analytical Laboratories. 13 Delta Dr. #4 Londonderry, NH 03053.
[30] Bursill LA, Hyde BG. Prog Solid State Chem 1972;7:177.